Elucidating the Performance Limitations of a 25 cm^2 Pure-Water-Fed Non-Precious Metal Anion Exchange Membrane Electrolyzer Cell

Michelle Sophie Lemcke,[a, b] Stefan Loos,[c] Nadine Menzel,[a] and Michael Bron*[b]

Anion exchange membrane (AEM) water electrolysis has emerged as a promising technology for producing hydrogen in a carbon-neutral economy. To advance its industrial application, performance evaluations of non-precious metal AEM electrolyzers with electrode areas of 25 cm^2 were conducted. The focus was on pure water operation, achieving a current density of 0.26 A cm^{-2} at a voltage of 2.2 V. To gain a better understanding, the AEM electrolyzer was also operated in aqueous KOH, yielding 1.2 A cm^{-2} at 2.2 V. By adding a liquid electrolyte and by varying cell components, causes of the occurring performance limitations and ways to improve the AEM electrolyzer were identified. Electrochemical impedance analysis showed that the activation loss at the anode due to sluggish OER kinetics was the limiting factor at low current densities. At higher current densities, which is the operating range of interest for industrial application, the ohmic resistance from the membrane was the dominant factor limiting high performance in pure water operation.

Introduction

Hydrogen gas serves as a crucial raw material for various industrial processes including the production of chemicals, steel and fertilizer. It also plays an important role in transport and energy storage, contributing to the reduction of CO_2 emissions. To achieve a climate-neutral economy, hydrogen production must be free of CO_2 emissions. One prevalent approach is through water electrolysis powered by renewable sources like wind and solar energy. In 2023, only about 0.1% of global hydrogen production came from water electrolysis,[1] while the rest was obtained from fossil fuels resulting in enormous CO_2 emissions. To meet the global demand for hydrogen solely through water electrolysis, the operating and capital costs of electrolyzers need to be decreased to install the required electrolyzer capacities. Although the proton exchange membrane (PEM) electrolysis and the alkaline electrolysis (AEL) are established technologies, they (currently) have limitations restricting the scale-up.[1,2]

Combining the benefits of AEL and PEM electrolysis, anion exchange membrane (AEM) water electrolysis has emerged as a promising technology with the potential for efficient and cost-effective hydrogen production.[2–6] A schematic of AEM electrolysis is presented in Figure 1. The anion-selective membrane, typically consisting of quaternary ammonium hydroxide groups bonded to a base polymer,[7] separates the electrodes. Hydroxide ions are transferred through the AEM from cathode to anode, balanced by the electrons flowing through an external circuit when a voltage is applied between the electrodes. At the cathode, water is split into hydrogen and hydroxide ions by accepting electrons. This process is the hydrogen evolution reaction (HER):
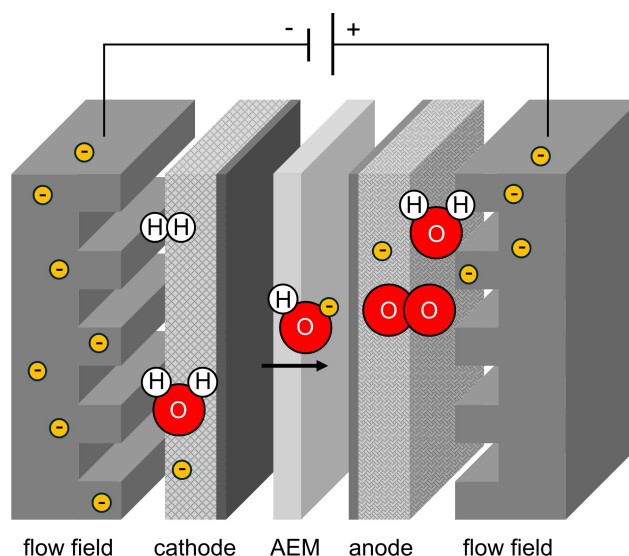
[a] M. S. Lemcke, Dr. N. Menzel
     Fraunhofer Institute for Wind Energy Systems IWES,
     Am Seedeich 45, 27572 Bremerhaven, Germany

[b] M. S. Lemcke, Prof. Dr. M. Bron
     Martin Luther University Halle-Wittenberg, Institute of Chemistry,
     Von-Danckelmann-Platz 4, 06120 Halle (Saale), Germany
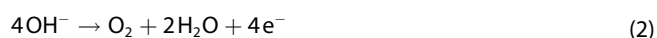   E-mail: michael.bron@chemie.uni-halle.de

[c] Dr. S. Loos
     Fraunhofer Institute for Manufacturing Technology and Advanced Materials
     IFAM, Winterbergstraße 28, 01277 Dresden, Germany

Figure 1. Schematic of anion exchange membrane (AEM) water electrolysis with catalyst coated porous transport layers (PTLs).

flow field   cathode   AEM   anode   flow field

ChemElectroChem

Research Article
doi.org/10.1002/celc.202400334

Chemistry
Europe

European Chemical
Societies Publishing

$$2H_2O + 2e^- \rightarrow H_2 + 2OH^-$$ (1)

The oxygen evolution reaction (OER) occurs at the anode releasing electrons:

$$4OH^- \rightarrow O_2 + 2H_2O + 4e^-$$ (2)

The OER is kinetically unfavorable due to the four-electron process and the nature of the O_2 formation causing a high overpotential.

Thus, the overall reaction is:

$$2H_2O \rightarrow O_2 + 2H_2$$ (3)

AEM electrolysis offers a compact zero-gap cell design due to the polymer membrane enabling variable-load and pure water operation. This is beneficial for coupling with intermittent power sources like renewable energies. Another advantage of AEM electrolysis is the use of inexpensive materials like non-precious metal catalysts due to the alkaline environment. However, AEM technology is still under development. Challenges are the stability and conductivity of membranes and ionomers, especially when operated in pure water. Improving the ionic conductivity usually involves increasing the water uptake and solubility of the membrane. However, this can cause swelling and softening of the AEM, which in turn reduces its stability.[8–12] Consequently, a lower ionic conductivity is often traded for the required mechanical stability in electrolyzers. Most studies on AEM electrolysis use an additional liquid electrolyte based on hydroxides or carbonates that conceals these conductivity and stability issues, particularly of the ionomer in the oxidative environment at the anode.[13,14] Only a few reported AEM electrolyzers operate solely with pure water. Most of them show limited durability of only a few hundred hours and low current densities.[3,4,7,15] Recent studies[13,16–18] provide more competitive performance in pure water with current densities of $1\,A\,cm^{-2}$ below a cell voltage of 2 V. However, they typically utilize precious metal catalysts to achieve high performance and operate in very small cells with electrode areas of 1 cm^2 to 5 cm^2. Exceptions are the studies by Li et al.[19] and Zheng et al.,[20] yielding $1\,A\,cm^{-2}$ at around 1.8 V using specialized NiFe- and NiMo-based electrodes operated in pure water but at elevated temperatures of 85 °C and 80 °C respectively to attain high performance. Although Li et al.[19] employed non-precious metal catalysts, a closer look reveals that they did not work entirely without precious metals, as the gas diffusion layer and flow field at the anode were coated with platinum. These findings indicate another challenge of the AEM technology regarding the catalysts and electrodes. There is a lack of research on stable and high-performing non-precious metal catalysts in pure water, particularly under industrially relevant conditions. This requires transitioning from half-cell and lab-scale testing with electrode areas of a few square centimeters to application-oriented conditions and sizes.

To advance in industrially relevant AEM electrolyzers, it is necessary to gain more insight into the factors limiting high performance and durability. Therefore, this study focuses on performance evaluations of membrane electrode assemblies (MEAs) under application-oriented conditions. The AEM electrolysis cells contain non-precious metal MEAs with electrode areas of 25 cm^2 and are operated with pure water at 60 °C. To gain a better understanding, measurements are also performed in low concentrated KOH solutions of 0.1 M KOH and 1 M KOH. Polarization curves and electrochemical impedance spectroscopy (EIS) are conducted to determine the performance losses and relate them to individual cell components. Reasons for these losses are identified to derive ways to improve and optimize the AEM electrolysis cell. By analyzing and understanding the MEA performance, we aim to contribute to the development of more efficient AEM electrolyzers.

Results and Discussion

The developed non-precious metal membrane electrode assembly (MEA) consists of a new membrane developed by Fumatech BWT GmbH placed between two electrodes with a geometrical area of 25 cm^2. The anode is made of copper-cobalt-manganese-oxide on a nickel powder-coated stainless-steel felt. Nickel was deposited on the stainless-steel substrate prior to applying the catalyst to increase the surface area for a higher catalyst utilization. The cathode is composed of Raney-Nickel on carbon paper. The MEA was operated in pure water and also in 0.1 M KOH and 1 M KOH to examine and understand the electrochemical behavior. The test protocol including polarization curves and electrochemical impedance spectroscopy (EIS) was performed at 60 °C and atmospheric pressure (see also Section "Experimental").

The recorded polarization curves are presented in Figure 2a giving insight into the occurring overvoltages due to ohmic, activation and mass transport losses. The rate of hydrogen production is expressed by the current density, while the voltage serves as the driving force for the electrolysis reaction.

In pure water, the MEA delivers a current density of $0.26\,A\,cm^{-2}$ at a voltage of 2.2 V. However, it yields a current density of $0.68\,A\,cm^{-2}$ in 0.1 M KOH and $1.2\,A\,cm^{-2}$ in 1 M KOH at the same voltage. Thus, the performance is more than doubled and quadrupled respectively by using low concentrated KOH solutions. As the cells use the same electrodes, membrane, flow field and end plates as well as clamping force, the improvement can be only attributed to the KOH solution. It influences the cell voltage already at $0.005\,A\,cm^{-2}$, i.e. in the region where the reactions at the electrodes start to proceed. The KOH-fed electrolyzers display a voltage of 1.47 V at $0.005\,A\,cm^{-2}$, while the pure-water-fed one exhibits a higher voltage of 1.66 V at the same current density. This is caused by higher activation overvoltages, as a higher activation energy is required for the reactions in pure water. This higher activation energy is also reflected in higher Tafel slopes (see Supporting Information). The significant performance improvement in KOH therefore arises from a higher catalytic activity of the electrodes resulting in lower activation overvoltages and from a higher ionic conductivity in the MEA resulting in a lower ohmic
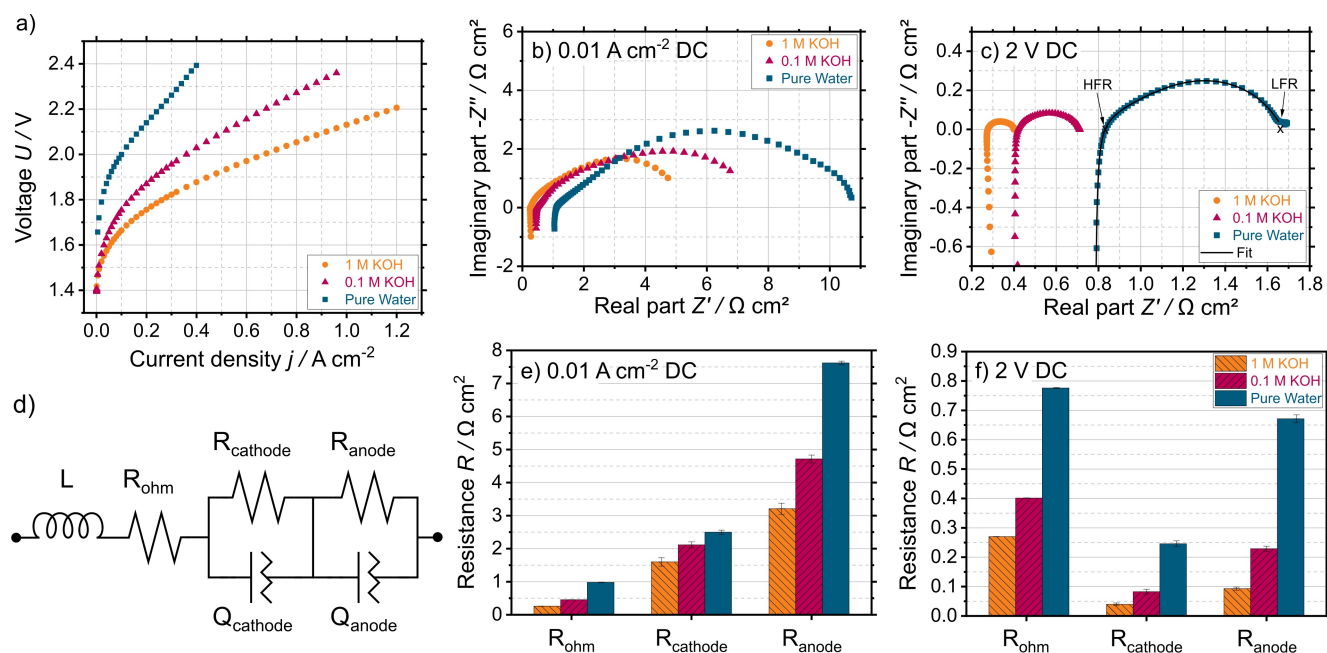
Figure 2. a) Polarization curves of the developed non-precious metal MEA with an electrode area of 25 cm^2 operated in pure water, 0.1 M KOH and 1 M KOH at 60 °C as well as EIS analysis using Nyquist plots from 100 kHz to 100 mHz at b) 0.01 A cm^{-2} and c) 2 V, d) the applied equivalent circuit model and thus obtained resistances at e) 0.01 A cm^{-2} and f) 2 V.

overvoltage. This is illustrated as the linear part of the polarization curve above 0.1 A cm^{-2} for pure water and 0.3 A cm^{-2} for KOH in Figure 2a.

These findings are supported by EIS analysis shown as Nyquist plots at 0.01 A cm^{-2}, close to the open circuit voltage (OCV), and at 2 V in Figure 2b and 2c. EIS at 2 V represents the area of the polarization curve at which the curve runs linearly determined by ohmic losses. However, EIS at 0.01 A cm^{-2} represents the kinetically dominated area of the polarization curve at low current densities. This part is attributed to the kinetic resistances resulting from the activation energy required for the reactions at the electrodes. As marked in Figure 2c, the intersection with the x-axis at high frequencies on the left-hand side of the Nyquist plot is the high frequency resistance (HFR). The HFR includes the ohmic resistance. Accordingly, the low frequency resistance (LFR) is the intersection with the x-axis at low frequencies on the right-hand side of the Nyquist plot. The LFR includes all contributions to the resistance, such as ohmic, activation and mass transport resistance. As shown in Figure 2b and 2c, the semicircle shape changes considerably and the HFR and LFR decrease significantly by adding aqueous KOH. Adding KOH solution increases the conductivity of the electrolyte that impacts both HFR and LFR. The influence of electrolyte conductivity on HFR is more direct and pronounced than on LFR, as the electrolyte resistance accounts for a major part of HFR, whereas it has a minor contribution to LFR. At low frequencies, other factors such as electrode kinetics and diffusion processes play a more significant role. In pure water, the highest HFR and LFR are observed both at 0.01 A cm^{-2} and 2 V, whereas they are the lowest for 1 M KOH.

To analyze the EIS plots in more detail, the EIS data was fitted with the equivalent electric circuit model schematized in Figure 2d. The model was derived from the physical processes of this non-precious metal electrolysis cell system. It consists of a series connection of an inductor (L), an ohmic resistance (R_{ohm}) and two parallel connections of a resistance and a constant phase element (CPE). Two are included in the model because of the elongated semicircle displayed in Figure 2b and 2c indicating two strongly overlapping semicircles. The resistances of the parallel connections represent the activation losses at the anode (R_{anode}) and cathode ($R_{cathode}$) due to the kinetics of the oxygen evolution reaction (OER) and the hydrogen evolution reaction (HER) respectively. This assignment is verified below (see Figure 4). R_{anode} and $R_{cathode}$ incorporate the charge transfer resistances of the reactions and equal the diameter of the semicircle in the Nyquist plot. The CPEs are attributed to the double layer capacitance at the cathode ($Q_{cathode}$) and anode (Q_{anode}). CPEs were chosen instead of capacitances since the system often does not behave ideally. R_{ohm} originates from the current flow through the cell and includes the ionic, electrical and contact resistances of all cell components. It equals the HFR. The inductor L characterized by positive imaginary parts represents inductive parts of the system, mainly of cables and wires, that occur at high frequencies. As displayed in Figure 2c, the Nyquist plot for pure water at 2 V shows a small tail at very low frequencies. This can be attributed to mass transport losses. In the research of Razmjooei et al.,[21] these losses were included as an additional resistor-CPE element in the equivalent circuit. However, in this work mass transport losses were not added as a third resistor-CPE element in the model due to insufficient data sets and data points related to them at the analyzed

ChemElectroChem

Research Article
doi.org/10.1002/celc.202400334

Chemistry Europe
European Chemical
Societies Publishing

operating points at 0.01 A cm^{-2} and 2 V. The resistances obtained by fitting the EIS data with the described equivalent circuit model are visualized in Figure 2e and 2f. The curve fit is exemplified in Figure 2c for the pure water operation.

At 0.01 A cm^{-2} in the kinetically dominated area, the activation resistance at the anode R_{anode} contributes most to the losses as illustrated in Figure 2e. R_{anode} is about three times higher in pure water and more than twice as high in aqueous KOH compared to the activation resistance at the cathode $R_{cathode}$. This shows that the OER is more strongly kinetically inhibited than the HER, in both pure water and KOH. Additionally, it confirms that the OER is kinetically unfavorable due to the four-electron process and the nature of the O_2 formation (see Eq. (2)). At the anode, four electrons are required to produce one molecule of oxygen, while only two electrons are needed at the cathode to produce one molecule of hydrogen. Thus, the OER is the rate-determining step and limiting factor of the electrolysis at low current densities.

Comparing the three differently fed MEAs, the MEA operated in pure water exhibits the highest R_{anode} and $R_{cathode}$ with $7.6 \ \Omega \text{cm}^2$ and $2.5 \ \Omega \text{cm}^2$ respectively at 0.01 A cm^{-2}. The lowest activation resistances are obtained for the MEA operated in 1 M KOH with $3.2 \ \Omega \text{cm}^2$ for R_{anode} and $1.6 \ \Omega \text{cm}^2$ for $R_{cathode}$. The MEA operated in 0.1 M KOH delivers intermediate activation resistances. This demonstrates that R_{anode} and $R_{cathode}$ are lower for KOH than for pure water operation. The same trend applies to the activation resistances at 2 V (see Figure 2f). These results emphasize that the reactions are less kinetically sluggish in KOH than in pure water. This confirms the higher catalytic activity of the electrodes due to the high pH resulting from the KOH solution. The activation enhancement is also related to the increased utilization of the catalyst layers due to the high hydroxide concentration in the liquid electrolyte leading to faster kinetics and more reaction sites. When operating in pure water, the ion transfer between membrane and electrode can only occur through direct contact of the AEM and catalyst particles as well as through direct contact of the AEM and the ionomer that is connected to catalyst particles (see Figure 3 (left)). However, when aqueous KOH is fed to the AEM electrolyzer, the high concentration of hydroxide ions in the liquid electrolyte provides additional ion transport pathways. Thus, reactions can also take place on catalyst surfaces that are not connected with ionomer (see Figure 3 (right)). Therefore, using KOH solutions leads to less kinetically inhibited reactions which explains the significant improvement. Consequently, these findings indicate that increasing the catalyst utilization is a way to reduce activation losses in pure water operation. This can be achieved by improving the catalyst and ionomer distribution through optimizing catalyst loading, ionomer content and catalyst application, as demonstrated in recent work.[22–26] Another option is to increase the electrochemically active surface area (ECSA) either by modifying the substrate surface or by incorporating a catalyst support like 2D transition metal carbides MXenes[27] to increase the inner surface of the catalyst layer. These enhancement approaches are particularly relevant for the anode, as the OER is the limiting factor at low current densities.
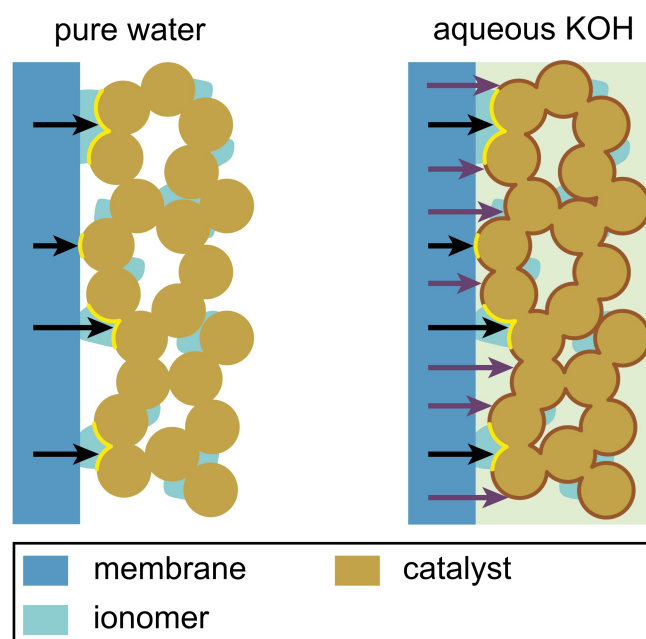

pure water   **aqueous KOH**

■ membrane   ■ catalyst
■ ionomer

Figure 3. Schematic of the ion transport at the interface of membrane and anode when the AEM electrolyzer is operated with pure water (left) and aqueous KOH (right). The yellow bold lines highlight the interface between catalyst and ionomer/AEM. The brown bold lines mark the interface between catalyst and liquid electrolyte. Black arrows illustrate the ion pathways between AEM and catalyst in direct contact and in contact through ionomer. Purple arrows represent additional ion pathways through the liquid electrolyte.

At 2 V in the ohmically dominated area, the ohmic resistance R_{ohm} contributes most to the losses as displayed in Figure 2f. As the increase in voltage enhances reaction kinetics and reduces the activation energy required for the electrochemical reactions, the activation resistances are reduced and lower than the ohmic resistance at 2 V. R_{ohm} is the highest for pure water with $0.78 \ \Omega \text{cm}^2$ at 2 V, while it is the lowest for 1 M KOH with $0.27 \ \Omega \text{cm}^2$. This is a decrease of 66 % at 2 V for 1 M KOH compared to pure water. For 0.1 M KOH, R_{ohm} is intermediate ($0.40 \ \Omega \text{cm}^2$) while being closer to that of 1 M KOH. The same trend applies to R_{ohm} at 0.01 A cm^{-2} (see Figure 2e). This confirms the higher ionic conductivity due to a higher amount of hydroxide ions from the KOH solution leading to a lower R_{ohm} in KOH. Consequently, these findings indicate that the ionic resistance has the largest impact on the ohmic resistance in pure water operation. Thus, the ohmic resistance of the membrane is the limiting factor of the pure-water-fed electrolyzer at 2 V. As this operating point is relevant for industrial application, it is crucial to minimize the occurring losses and overcome performance limitations. In addition to ohmic losses, the activation losses at the anode contribute significantly to the performance limitations in pure water operation at 2 V. Approaches to reduce R_{anode} by increasing the catalyst utilization were presented above. A way to reduce R_{ohm} in pure water operation is to increase the ionic conductivity of the AEM. As previously stated, increasing the ionic conductivity often leads to a decrease of stability. This observation under-

ChemElectroChem

Research Article
doi.org/10.1002/celc.202400334

Chemistry
Europe
European Chemical
Societies Publishing

lines the importance of developing advanced membranes and ionomers with high ionic conductivity and high stability. A less challenging alternative is to use an additional source of hydroxide ions like aqueous KOH. The results show that feeding 0.1 M KOH to the electrolyzer significantly reduces both ohmic and activation losses and thus considerably increases the performance compared to pure water operation. The higher efficiency of the KOH-fed AEM electrolyzer directly correlates with reduced costs compared to the pure-water-fed one. Since 0.1 M or even further diluted KOH is less corrosive, this appears to be a reasonable compromise between high efficiency and simple system engineering.

To validate the equivalent circuit model and differentiate the contributions of anode and cathode, the AEM electrolysis cell was varied by replacing the non-precious metal HER catalyst Raney-Nickel with platinum on carbon. Since a different cell set-up had to be used for the platinum cathode, the tests with the non-precious metal MEA were repeated. This was necessary to ensure comparability by only changing the cathode and no other component. Thus, all other components like anode, membrane, flow field and end plates as well as the test protocol and procedures prior to testing stayed the same.

The polarization curves of the MEAs with platinum cathode and those with nickel cathode operated in pure water and in 1 M KOH are displayed in Figure 4a. The abbreviations used are defined as follows: MEA Pt-KOH refers to the MEA with platinum cathode operated in 1 M KOH, MEA Ni-KOH refers to the MEA with nickel cathode operated in 1 M KOH, MEA Pt-W refers to the MEA with platinum cathode operated in pure water, and MEA Ni-W refers to the MEA with nickel cathode operated in pure water. The MEA Pt-KOH achieves the best performance, whereas the MEA Ni-W performs the poorest. At 2.2 V, the MEAs

with platinum deliver current densities of 1.30 A cm^{-2} in KOH and 0.55 A cm^{-2} in pure water and the MEAs with Raney-Nickel 0.82 A cm^{-2} in KOH and 0.41 A cm^{-2} in pure water. The results demonstrate that the MEAs with platinum as HER catalyst perform twice as well (in pure water and in KOH) as the non-precious metal MEAs. Furthermore, it shows that the MEAs perform in 1 M KOH two to three times better than in pure water. At 0.005 A cm^{-2}, i.e. in the region where the reactions at the electrodes start to proceed, the voltage is 0.1 V lower for KOH than for pure water and somewhat (0.015 V) lower for platinum than for nickel.

To gain deeper insight into the system, EIS was carried out. The Nyquist plots at 0.01 A cm^{-2} and 2 V as well as the obtained resistances by fitting with the equivalent circuit described above (see Figure 2d) are presented in Figure 4. The EIS data agrees with the polarization curves: The poorly performing MEAs have high resistances and the well-performing MEAs have low resistances. As visualized in Figure 4e, the ohmic resistance R_{ohm} is the highest among all losses and thus the limiting factor at 2 V in the industrially relevant operating range. MEAs Pt-KOH, Ni-KOH, Pt-W and Ni-W attain R_{ohm} of 0.35 Ω cm^2, 0.41 Ω cm^2, 0.55 Ω cm^2 and 0.57 Ω cm^2 respectively. As previously discussed, R_{ohm} is higher for operation in pure water than in KOH due to a lower ionic conductivity in pure water. Additionally, the data demonstrates that R_{ohm} is lower for platinum than for Raney-Nickel. This is caused by the higher electrical conductivity of the platinum on carbon catalyst. Comparing the influence of the electrolyte to that of the HER catalyst, the improvement of the ionic resistance has a greater impact on R_{ohm} than that of the electrical resistance.

Shifting the focus to low current densities, Figure 4d illustrates that the activation losses at the anode are the limiting
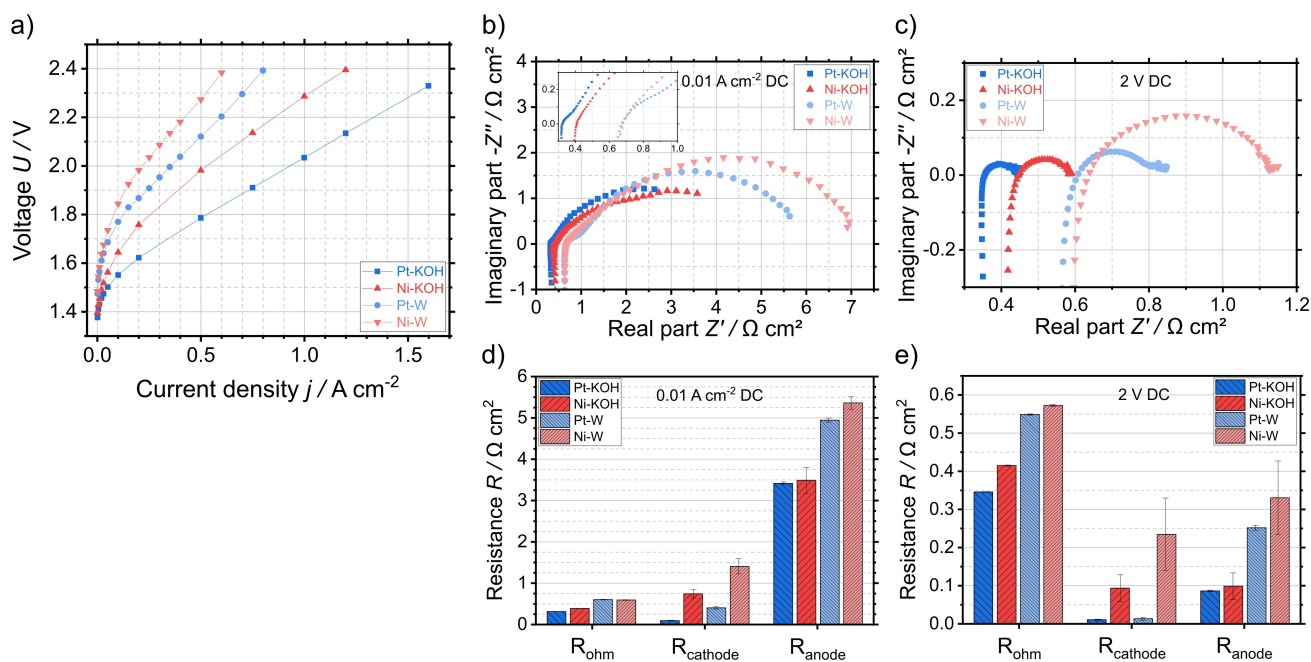

Figure 4. a) Polarization curves of the developed MEAs with platinum cathode and nickel cathode with an electrode area of 5 cm^2 operated in pure water and 1 M KOH at 60 °C as well as EIS analysis using Nyquist plots from 100 kHz to 100 mHz at b) 0.01 A cm^{-2} (with a magnified Nyquist plot shown in the inset) and c) 2 V and resistances at d) 0.01 A cm^{-2} and e) 2 V obtained by fitting with the equivalent circuit.

ChemElectroChem

Research Article
doi.org/10.1002/celc.202400334

**Chemistry
Europe**
European Chemical
Societies Publishing

factor of the electrolysis at 0.01 A cm^{-2}. This agrees with the previous findings discussed in more detail above. R_{anode} falls within the same range for MEAs operated in KOH with 3.4 Ω cm^2 for MEA Pt-KOH and 3.5 Ω cm^2 for MEA Ni-KOH, as well as for MEAs operated in pure water with 5.0 Ω cm^2 for MEA Pt-W and 5.4 Ω cm^2 for MEA Ni-W at 0.01 A cm^{-2}. Since all four MEAs consist of the same anode, the major differences arise from the addition of a liquid electrolyte and thus from the higher catalytic activity in aqueous KOH. However, small differences between same electrodes in same medium can occur due to the strongly porous structure of the electrodes. Therefore, the specific ECSA may somewhat differ, especially in small cells with 5 cm^2 electrodes. The differences may be less pronounced for larger electrode areas, as it averages out. Another reason may be fit inaccuracies due to strongly overlapping semicircles for the non-precious metal MEAs appearing as error bars in Figure 4d and 4e.

Furthermore, an interesting aspect to examine is the effect of the cathode on the impedance and cell performance. By replacing the non-precious metal cathode with a platinum one, the semicircles attributed to the activation losses can be more clearly distinguished from each other in the Nyquist plot. As displayed in the magnified Nyquist plot in the inset of Figure 4b, the semicircle attributed to the activation losses of the cathode shifted slightly to higher frequencies. Thus, the semicircles overlap less in comparison to those of the MEAs with nickel cathode. This indicates that the platinum cathode enables faster HER kinetics. In addition, the activation resistance at the cathode $R_{cathode}$ is lower for platinum than for nickel as presented in Figure 4d. $R_{cathode}$ decreases by 87% at 0.01 A cm^{-2} from 0.7 Ω cm^2 to 0.1 Ω cm^2 in KOH and by 71% from 1.4 Ω cm^2 to 0.4 Ω cm^2 in pure water by using the platinum cathode instead of the nickel one. This results from the higher catalytic activity of the platinum catalyst leading to a lower activation energy that is required for the HER. Thus, the developed equivalent circuit model is confirmed since $R_{cathode}$ changes while R_{anode} remains in the same range when varying the cathode catalyst.

Moreover, Pt-W shows a long tail or even an additional small semicircle at very low frequencies related to mass transport losses. At a higher voltage like 2.2 V (see Figure S1 in the Supporting Information) the mass transport losses are visualized as a tail in 45° angle in the Nyquist plot indicating diffusion processes. These losses result from insufficient supply of water and hydroxide ions as well as from insufficient removal of excess water, hydrogen gas and oxygen gas. Mass transport losses in pure water operation can be addressed by enhancing the conductivity and porosity of the electrode. One approach to improve the porosity is to apply a microporous layer onto the substrate or porous transport layer, as demonstrated by Razmjooei et al.[21] This results in a mixture of small and large pores that is beneficial for the gas and fluid exchange.

Comparing to literature can be difficult due to differences in test setups, test protocols and operating parameters. Additionally, there is limited literature available on AEM electrolysis tests using non-precious metal MEAs with an electrode area of 25 cm^2 operated in pure water. Hence, we conducted electrol-

ysis tests using both the newly developed membrane and electrodes as well as commercially available ones for reference. Thus, four different MEAs with various configurations were assembled placing the developed membrane between the developed electrodes (MEA El-Mem), the developed membrane between the commercial electrodes (MEA RefEl-Mem), the commercial membrane between the commercial electrodes (MEA RefEl-RefMem) and the commercial membrane between the developed electrodes (MEA El-RefMem). One advantage of this approach is that the developed electrodes and membrane can be evaluated independently. The electrodes can be tested with commercially available membranes, and the membrane can be tested with commercially available electrodes. Figures 5 and 6a show the polarization curves of the four different MEAs using non-precious metal electrodes with an electrode area of 25 cm^2 operated at 60 °C and atmospheric pressure in pure water and in 1 M KOH respectively.

Large differences in performance can be seen for the operation in pure water (see Figure 5). MEA El-Mem achieves the best performance with 0.26 A cm^{-2} at a cell voltage of 2.2 V. However, the MEAs with the commercial electrodes RefEl-RefMem and RefEl-RefMem deliver the poorest performances with 0.02 A cm^{-2}. Thus, the performance of the developed MEA is 13 times higher at 2.2 V than that of the reference MEA. The reason for this is the low catalytic activity of the commercial electrodes in neutral media like pure water. These electrodes were designed for use in alkaline media, whereas the developed electrodes were optimized for pure water operation and are therefore active in neutral media. The other MEA configuration El-RefMem delivers a current density of 0.17 A cm^{-2} at 2.2 V. It must be added that the measurements with this MEA El-RefMem were very unstable and all five electrolysis tests with this MEA type failed after a short time due to short circuit. After disassembly, it was evident that the membrane cracked and thinned at the edge of the electrode area, indicating a lower mechanical stability (see Figure S2 in the Supporting Informa-
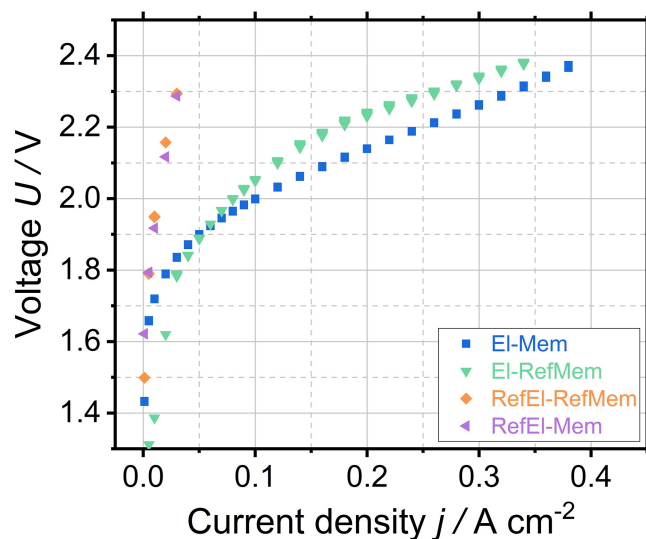

Figure 5. Polarization curves of four different non-precious metal MEAs with electrode areas of 25 cm^2 operated in pure water at 60 °C.

ChemElectroChem

Research Article
doi.org/10.1002/celc.202400334

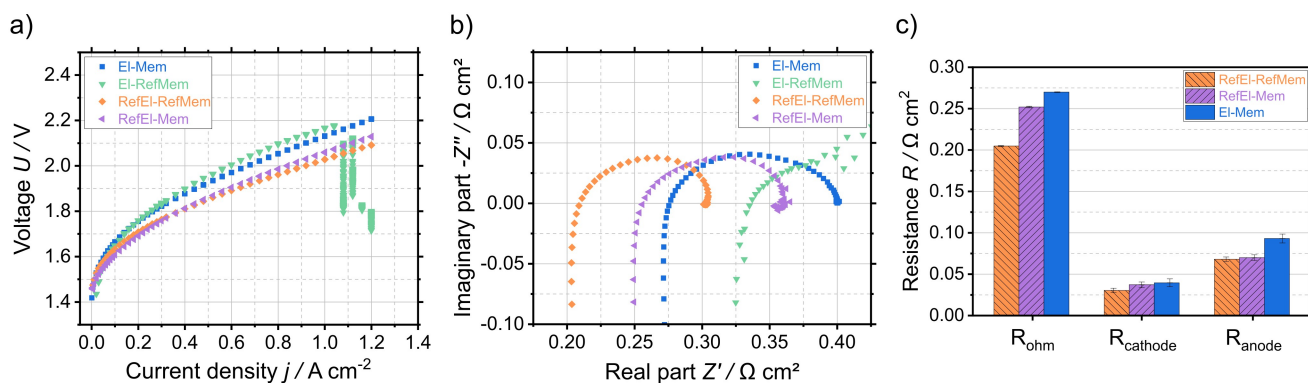**Chemistry
Europe**

European Chemical
Societies Publishing

Figure 6. a) Polarization curves of four different non-precious metal MEAs with electrode areas of 25 cm² operated in 1 M KOH at 60 °C as well as EIS analysis using. b) Nyquist plots from 100 kHz to 100 mHz at 2 V and c) resistances at 2 V obtained by fitting with the equivalent circuit (missing data for El-RefMem due to repeated cell failure).

tion). Therefore, no conclusions can be drawn regarding which membrane performs electrochemically better in pure water. In terms of mechanical stability, the developed membrane proved to be more robust and easier to handle than the commercially available one, particularly with thick electrodes (e.g. 750 μm thick anode). The findings are confirmed by EIS (see Figure S3 in the Supporting Information).

Operating in 1 M KOH (see Figure 6a), the four different MEAs show a similar behavior. As in pure water operation, the curves of the MEAs with the same electrode type are closer together. Since the MEAs reached the maximum current limit of the potentiostat below 2.2 V, the MEA performance is discussed at 1 A cm⁻² in the following. The MEAs with the developed electrodes require the highest voltages with 2.17 V for El-RefMem and 2.13 V for El-Mem in 1 M KOH at a current density of 1 A cm⁻². However, the MEAs with the commercial electrodes attain the lowest voltages with 2.06 V for RefEl-RefMem and 2.03 V for RefEl-RefMem. Consequently, the reference MEA RefEl-RefMem achieves the best performance in 1 M KOH. Comparing to literature and manufacturer information stating 1.9 V at 1 A cm⁻²,[28] our measurement results are poorer. This may arise from differences in test setups, test protocols, operating parameters, electrode area size (5 cm² vs. 25 cm²) and materials batches.

Evaluating the membrane, the data shows that the developed membrane can compete with the commercially available one, as the differences in performance are minor for the MEAs RefEl-Mem and RefEl-RefMem with same electrodes and different membranes.

Moreover, Figure 6a visualizes the failure of the MEA El-RefMem above 1 A cm⁻² caused by short circuit. This leads to considerable instability in the EIS data (see Figure 6b) making it unsuitable for evaluation. Hence, the resistances of El-RefMem are not plotted in Figure 6c.

Figure 6b and 6c display the Nyquist plot at 2 V and the corresponding resistances obtained by fitting the data with the equivalent circuit described above (see Figure 2d). The EIS data reflects the findings of the polarization curves. RefEl-RefMem has the lowest ohmic resistance (0.20 Ω cm²) followed by RefEl-

Mem (0.25 Ω cm²) and El-Mem (0.27 Ω cm²). El-RefMem exhibits the highest HFR but this should be viewed with caution due to the short circuit. The findings indicate that RefEl-RefMem is associated with a high ionic and electrical conductivity as well as a low contact resistance. Differences in R_{ohm} between RefEl-RefMem and RefEl-Mem can be primarily attributed to the different membranes, with the developed membrane having a lower ionic conductivity. However, the ohmic resistances of RefEl-Mem and El-Mem are very close. The main reason is the use of the same membrane type and thus similar ionic conductivity. Differences may result from higher electrical resistances for El-Mem due to thicker electrodes. Consequently, utilizing thinner substrates may reduce the ohmic resistance. Reducing R_{ohm} is crucial as it is the primary contributor to losses at 2 V making it the limiting factor in the operating range of interest.

Comparing the activation losses at 2 V in Figure 6c, the reference MEA RefEl-RefMem has the lowest activation resistances with 0.07 Ω cm² and 0.03 Ω cm² for R_{anode} and $R_{cathode}$ respectively. The developed MEA El-Mem delivers the highest activation resistances with 0.09 Ω cm² and 0.04 Ω cm² for R_{anode} and $R_{cathode}$ respectively. RefEl-Mem exhibits intermediate activation resistances that are closer to those of RefEl-RefMem. Thus, the Nyquist plots in Figure 6b illustrate a similar shape for RefEl-RefMem and RefEl-Mem. Obviously, the same electrode type results in a similar kinetic behavior. Differences can be attributed to the membranes and ionomers: RefEl-RefMem is prepared with the same ionomer for the membrane and catalyst layer, whereas RefEl-Mem comprises different ionomers for the membrane and catalyst layer leading to a slightly higher charge transfer resistance. In contrast, El-Mem has a different shape and a larger semicircle diameter indicating higher activation resistances. Thus, Figure 6b and 6c demonstrate that the commercial electrodes catalyze the reactions better in 1 M KOH than the developed electrodes. The lower catalytic activity for the developed electrodes results from their design for reversible operation, as the selected catalysts are active in electrolysis mode (OER and HER) and in fuel cell mode (ORR

ChemElectroChem

Research Article
doi.org/10.1002/celc.202400334

**Chemistry
Europe**

European Chemical
Societies Publishing

and HOR). Electrodes developed specifically for the electrolysis may have achieved a higher catalytic activity.

Conclusions

In conclusion, the developed non-precious metal MEA was successfully operated in pure water at 60 °C, yielding a current density of 0.26 A cm^{-2} with 25 cm^2 electrode area and 0.41 A cm^{-2} with 5 cm^2 electrode area at a voltage of 2.2 V. This is one of the best reported performances using non-precious metal electrodes in pure water. It is only clearly surpassed by the above-mentioned study by Zheng et al.[20] operating at a considerably higher temperature of 80 °C.

The lower performance is partially related to our test setup, as the electrolysis tests with the commercially available MEA exhibited higher losses compared to the manufacturer information. Therefore, the examined MEAs may have performed better in a superior test bench. Additionally, the variation with commercially available electrodes, that demonstrated higher catalytic activity and lower activation resistances, indicated that the developed non-precious metal MEA may have achieved higher current densities with electrodes developed specifically for the electrolysis.

Furthermore, an electric circuit model for the analysis of the EIS data was successfully developed. It was validated by replacing the non-precious metal HER catalyst with platinum on carbon. EIS was used to determine the factors restricting high performance. At 2 V in the operating range of industrial application, the ohmic loss was the dominant limiting factor. The primary contributor to the ohmic loss was the ohmic resistance from the membrane in pure water operation. Although the developed AEM proved to be competitive with commercially available ones, it is suggested that the ionic conductivity of the AEM in pure water is further increased to enhance cell performance. Another significant limiting factor was the activation loss at the anode due to sluggish OER kinetics, particularly at low current densities.

Additionally, the performance evaluations showed that the electrode structure can be further improved. This involves enhancing its porosity indicated by the observed mass transport losses, and optimizing the catalyst and ionomer distribution to increase the catalyst utilization in pure water to reduce activation losses. Variations with the platinum cathode or the commercially available electrodes also revealed that the ohmic resistance can be reduced by applying catalysts with a higher electrical conductivity or by employing thinner substrates. Overall, EIS has proven to be a useful method for understanding and giving a deeper insight into the performance limitations of the electrolysis cell.

This work is limited to the initial performance of the AEM electrolyzer in the first five hours of operation. Degradation investigations and performance losses during extended operation will be discussed in a separate work.

Experimental

Membrane Electrode Assemblies

The developed non-precious metal electrodes were prepared by Fraunhofer IFAM in Dresden, Germany. The anode catalyst $Cu_{0.6}Mn_{0.3}Co_{2.1}O_4$ was synthesized adapting a procedure reported by Paknahad et al.[29] CuCoMn-precursors were precipitated with 2 mol L^{-1} NaOH as hydroxides and then oxidized at 300 °C in air for five hours. In a typical procedure: 5.758 g Cu(NO$_3$)$_2 \cdot$ 2.5 H$_2$O (24.8 mmol), 2.450 g MnCl$_2 \cdot$ 4 H$_2$O (12.4 mmol) and 25.220 g Co(NO$_3$)$_2 \cdot$ 6 H$_2$O (86.7 mmol) were dissolved in 500 mL water before NaOH solution was added dropwise with small excess of NaOH-lye. The precipitate was washed three times with deionized water and dried at room temperature under reduced pressure. The precursor was transferred to an oven for oxidation at 300 °C in air. The resulting dark black material has been analyzed by X-ray powder diffraction (see Figure S4 in the Supporting Information). The elemental fractions of $Cu_{0.6}Mn_{0.3}Co_{2.1}O_4$ were determined by inductively coupled plasma optical emission spectrometry (ICP-OES) after dissolving the catalyst (typically about 50 mg to 100 mg) in a mixture of hydrochloric acid (3 volume parts, about 12 mL) and nitric acid (1 volume part, about 4 mL). This resulted in a metal ratio of 20.5 % Cu (expected 21.4 %), 9.7 % Mn (expected 9.1 %) and 69.5 % Co (expected 69.5 %). The cathode catalyst Raney-Nickel was purchased from Gaskatel GmbH. Catalyst inks were fabricated using the ionomer FAA3 from Fumatech BWT GmbH (20 % ionomer content in relation to the sum of catalyst and ionomer weight), n-propanol as solvent and the respective catalyst. Electrodes of 25 cm^2 were produced by hand-spraying the catalyst inks onto substrates. Raney-Nickel was coated on carbon paper 36AA from SGL Carbon SE and $Cu_{0.6}Mn_{0.3}Co_{2.1}O_4$ on 316 L-fiber felt from Bekaert NV that was coated with nickel powder and sintered in inert gas prior to applying the catalyst. The estimated catalyst loading was 4 mg cm^{-2} derived from several experiments and based on mass difference before and after the coating of catalyst on the PTL. The thickness of the electrodes was about 250 μm for the cathode and 750 μm for the anode. Scanning electron microscopy (SEM) and energy dispersive X-ray (EDX) analysis of the $Cu_{0.6}Mn_{0.3}Co_{2.1}O_4$-coated modified 316 L-fiber felt is shown in Figure S5 in the Supporting Information.

The developed membrane was synthesized by Fumatech BWT GmbH. It is a polyaliphatic anion exchange membrane with a thickness of about 50 μm. Before testing, the AEM was immersed in 1 M KOH for 24 h (replaced after 8 h) for ion exchange and rinsed with ultra pure water (0.055 μS cm^{-1}). The developed membrane electrode assembly (MEA) was part of the project "REVAL" with the aim to develop an AEM stack for reversible operation. Therefore, the above described electrodes and membrane can be applied in electrolysis and fuel cell devices.

The platinum cathode electrodes were prepared by hand-spraying the catalyst ink onto carbon paper 39AA from SGL Carbon SE with a platinum loading of 1 mg cm^{-2}. The catalyst ink consisted of catalyst, FAA3 ionomer from Fumatech BWT GmbH (20 % ionomer content in relation to the sum of catalyst and ionomer weight) and ethanol as solvent. As catalyst, platinum on carbon black (HiSPEC® 4000) from Alfa Aesar was utilized, containing 40 % Pt.

As reference, electrodes and membranes were purchased from Dioxide Materials. Sustainion® X37-50 Grade RT was used as AEM. The anode consisted of NiFe$_2$O$_4$ hand-painted on stainless steel fiber paper and the cathode of NiFeCo on nickel fiber paper. The thickness of the anode was about 600 μm and the one of the cathode about 300 μm.

AEM Electrolyzer Tests

An in-house built test bench was used to perform the AEM electrolyzer tests. For all electrochemical measurements, the potentiostat/galvanostat Gamry Reference 3000 and the Gamry Reference 30 k booster were employed. MEAs were assembled in the commercially available 25 cm^2 electrolyzer test cell by Dioxide Materials (see Figure S6 in the Supporting Information). The cell consists of flow field and end plates made of titanium and stainless steel. For the cell tests with platinum cathodes, a 5 cm^2 test cell was used with Nickel plates. After installing the electrolyzer cell in the test bench, the system was heated up for 30 min circulating water or KOH solution. Test conditions were 60 °C and atmospheric pressure. The cell temperature was monitored with a thermocouple in the flow field plate of the anode. The cells were operated with pure water (0.055 μS cm^{-1}), 0.1 M KOH (pH 13) or 1 M KOH (pH 14) with feed flows of 80 mL min^{-1} for the 25 cm^2 cell and 50 mL min^{-1} for the 5 cm^2 cell. It was fed to the anode and the cathode. After one hour of activation at cell voltages of 1.8 V and 2.2 V, the AEM electrolyzer cells were characterized by recording polarization curves and electrochemical impedance spectroscopy (EIS). The polarization curves were conducted by step-wise increasing the current density until the maximum cell voltage of 2.4 V was reached. Each current density step was held for at least 2 min. EIS was carried out from 100 kHz to 100 mHz recording ten points per decade. It was conducted at 0.01 A cm^{-2}, 1.8 V, 2 V and 2.2 V with an amplitude of 0.005 A cm^{-2} and 0.01 V respectively. For the KOH-fed electrolyzer tests, EIS was also measured at 0.1 A cm^{-2} and 0.2 A cm^{-2} with an amplitude of 0.05 A cm^{-2}. The respective voltage or current density was held for 5 min prior to the EIS measurement. The electrolyzer tests were repeated to ensure reproducibility.

Conflict of Interests

The authors declare no conflict of interest.

Data Availability Statement

The data that support the findings of this study are available from the corresponding author upon reasonable request.

[1] IEA – International Energy Agency, Global Hydrogen Review 2023, can be found under https://www.iea.org/reports/global-hydrogen-review-2023 **2023**.
[2] K. Ayers, N. Danilovic, R. Ouimet, M. Carmo, B. Pivovar, M. Bornstein, *Annu. Rev. Chem. Biomol. Eng.* **2019**, *10*, 219.
[3] H. A. Miller, K. Bouzek, J. Hnat, S. Loos, C. I. Bernäcker, T. Weißgärber, L. Röntzsch, J. Meier-Haack, *Sustain. Energy Fuels* **2020**, *4*, 2114.
[4] I. Vincent, D. Bessarabov, *Renewable Sustainable Energy Rev.* **2018**, *81*, 1690.
[5] S. Peng, *Electrochemical Hydrogen Production from Water Splitting: Basic, Materials and Progress*, Springer Nature Singapore and Imprint Springer, Singapore, 1st ed. 2023 edition **2023**.
[6] C. Li, J.-B. Baek, *Nano Energy* **2021**, *87*, 106162.
[7] D. Henkensmeier, M. Najibah, C. Harms, J. Žitka, J. Hnát, K. Bouzek, *Journal of Electrochemical Energy Conversion and Storage* **2021**, *18*.
[8] M. Mandal, G. Huang, P. A. Kohl, *ACS Appl. Energ. Mater.* **2019**, *2*, 2447.
[9] W. Chen, M. Mandal, G. Huang, X. Wu, G. He, P. A. Kohl, *ACS Appl. Energ. Mater.* **2019**, *2*, 2458.
[10] J. Fan, S. Willdorf-Cohen, E. M. Schibli, Z. Paula, W. Li, T. J. G. Skalski, A. T. Sergeenko, A. Hohenadel, B. J. Frisken, E. Magliocca, W. E. Mustain, C. E. Diesendruck, D. R. Dekel, S. Holdcroft, *Nat. Commun.* **2019**, *10*, 2306.
[11] G. Huang, M. Mandal, N. U. Hassan, K. Groenhout, A. Dobbs, W. E. Mustain, P. A. Kohl, *J. Electrochem. Soc.* **2020**, *167*, 164514.
[12] G. Huang, M. Mandal, N. U. Hassan, K. Groenhout, A. Dobbs, W. E. Mustain, P. A. Kohl, *J. Electrochem. Soc.* **2021**, *168*, 024503.
[13] G. A. Lindquist, S. Z. Oener, R. Krivina, A. R. Motz, A. Keane, C. Capuano, K. E. Ayers, S. W. Boettcher, *ACS Appl. Mater. Interfaces* **2021**, *13* (44), 51917.
[14] G. A. Lindquist, J. C. Gaitor, W. L. Thompson, V. Brogden, K. J. T. Noonan, S. W. Boettcher, *Energy Environ. Sci.* **2023**, *16*, 4373.
[15] Y. Leng, G. Chen, A. J. Mendoza, T. B. Tighe, M. A. Hickner, C.-Y. g, *J. Am. Chem. Soc.* **2012**, *134*, 9054.
[16] W. Song, K. Peng, W. Xu, X. Liu, H. Zhang, X. Liang, B. Ye, H. Zhang, Z. Yang, L. Wu, X. Ge, T. Xu, *Nat. Commun.* **2023**, *14*, 2732.
[17] R. Soni, S. Miyanishi, H. Kuroki, T. Yamaguchi, *ACS Appl. Energ. Mater.* **2021**, *4*, 1053.
[18] J. Xiao, A. M. Oliveira, L. Wang, Y. Zhao, T. Wang, J. Wang, B. P. Setzler, Y. Yan, *ACS Catal.* **2021**, *11*, 264.
[19] D. Li, E. J. Park, W. Zhu, Q. Shi, Y. Zhou, H. Tian, Y. Lin, A. Serov, B. Zulevi, E. D. Baca, C. Fujimoto, H. T. Chung, Y. S. Kim, *Nat. Energy* **2020**, *5*, 378.
[20] Y. Zheng, A. Serban, H. Zhang, N. Chen, F. Song, X. Hu, *ACS Energy Lett.* **2023**, *8* (12), 5018–5024.
[21] F. Razmjooei, T. Morawietz, E. Taghizadeh, E. Hadjixenophontos, L. Mues, M. Gerle, B. D. Wood, C. Harms, A. S. Gago, S. A. Ansar, K. A. Friedrich, *Joule* **2021**, *5*, 1776.
[22] S. Koch, P. A. Heizmann, S. K. Kilian, B. Britton, S. Holdcroft, M. Breitwieser, S. Vierrath, *J. Mater. Chem. A* **2021**, *9*, 15744.
[23] S. Koch, L. Metzler, S. K. Kilian, P. A. Heizmann, F. Lombeck, M. Breitwieser, S. Vierrath, *Adv. Sustainable Syst.* **2023**, *7*, 2200332.
[24] Y. S. Park, M. J. Jang, J.-Y. Jeong, J. Lee, J. Jeong, C. Kim, J. Yang, S. M. Choi, *Int. J. Energy Res.* **2023**, *2023*, 1.
[25] L. Wan, J. Liu, Z. Xu, Q. Xu, M. Pang, P. Wang, B. Wang, *Small (Weinheim an der Bergstrasse, Germany)* **2022**, *18*, e2200380.
[26] X. Zhang, Y. Li, W. Zhao, J. Guo, P. Yin, T. Ling, *Int. J. Minerals Metallurgy Materials* **2023**, *30*, 2259.
[27] Y. S. Park, A. Chae, G. H. Choi, S. Ram, S.-C. Lee, S. Bhattacharjee, J. Jung, H. S. Jeon, C.-H. Ahn, S. S. Hwang, D.-Y. Koh, I. In, T. Oh, S. J. Kim, C. M. Koo, A. S. Lee, *Applied Catalysis B: Environmental* **2024**, *346*, 123731.
[28] Z. Liu, S. D. Sajjad, Y. Gao, H. Yang, J. J. Kaczur, R. I. Masel, *Int. J. Hydrogen Energy* **2017**, *42*, 29661.
[29] P. Paknahad, M. Askari, M. Ghorbanzadeh, *Appl. Phys. A* **2015**, *119*, 727.